Eur. Phys. J. D **41**, 163–170 (2007)
DOI: 10.1140/epjd/e2006-00195-x

THE EUROPEAN PHYSICAL JOURNAL D

Finite number of vortices and bending of finite vortex lines in a confined rotating Bose-Einstein condensate

Z.Z. Chen and Y.L. Ma[a]

Department of Physics, Fudan University, Shanghai 200433, P.R. China

Received 16 August 2005 / Received in final form 14 April 2006
Published online 1st September 2006

Abstract. The minimal energy configurations of finite N_v-body vortices in a rotating trapped Bose-Einstein condensate is studied analytically by extending the previous work [Y. Castin, R. Dum, Eur. Phys. J. D **7**, 399 (1999)], and taking into account the finite size effects on z-direction and the bending of finite vortex lines. The calculation of the energy of the vortices as a function of the rotation frequency of the trap gives number, curvature, configuration of vortices and width of vortex cores self-consistently. The numerical results show that (1) the simplest regular polynomial of the several vortex configurations is energetically favored; while the hexagonal vortex lattice is more stable than square lattice; (2) bending is more stable then straight vortex line along the z-axis for $\lambda < 1$; (3) the boundary effect is obvious: compared with the estimation made under infinite boundary, the finite size effect leads to a lower vortex density, while the adding vortex bending results in a less higher density because of the expansion. The results are in well agreement with the other authors' ones.

PACS. 03.75.Lm Tunneling, Josephson effect, Bose-Einstein condensates in periodic potentials, solitons, vortices and topological excitations – 32.80.Pj Optical cooling of atoms; trapping

1 Introduction

Vortices (in two spatial dimensions, 2D) and vortex lines (in three spatial dimensions, 3D) are formed in a Bose-Einstein condensate (BEC) by stirring the trapped BEC with laser beam. Depending on the angular frequency (Ω) of the stirring beam, it is possible to generate configurations with different numbers of vortices (N_v) which form finite-size crystallization with different structures. In the past few years, vortex experiments in the trapped BEC have ranged from the study of individual or few vortices [1–4] and vortex rings [5,6] to the study of vortex lattices [7–11]. Various theoretical studies have been made in the field of many-body physics based on Gross-Pitaevskii (GP) mean-field model by a single macroscopic wave function $\Psi(\mathbf{r}) = |\Psi(\mathbf{r})|e^{i\phi(\mathbf{r})}$, imposing strong constraints upon its velocity field $\boldsymbol{v} = \hbar\nabla\phi/M$ (for a review, see, for example, [12]; for some fundamental concepts, see, for example, [13]). Theoretical investigations of vortex stability have been previously restricted to the case of a single vortex, either from a purely analytical point of view, such as in [14–16]; or by mixing analytical and numerical techniques [17–19]. The static and dynamic properties of the trapped BEC with the vortex lattice [20–26] as well as vortex lattices of spinor, multicomponent condensates [27–29] and multiquantum vortices [30] have being under extensive theoretical study. The presence of melting of the vortex lattice [31,32] and stripes of the vortex array [33,34] has also being investigated. Theoretical approaches in nonlinear dynamics [35–39] help us to understand the formation process of the vortex lattice in short- [33] and long- [10] lived regions. A U- or S-shaped vortex (bending and derivation from the center) has been observed under a certain Ω at different times [40,41]. Bent vortices were first studied numerically in [42,43] and analytically in [44], including the vortex shapes, configurations and energy diagram [45,46]. For describing the final equilibrium state, there have been several theoretical attempts [47–50], much attention focus on the effects of finite vortex number and condensate size numerically. However, the total energy functional for the vortex lines are still more complicated [44,45,51] when taking into account the effect of the shape of the vortex lines. The aim of this work, in analytical means, is to clearly understand the stationary configurations of the BEC rotating at a frequency Ω with finite number of vortices and bending of finite vortex lines located within finite sizes both in the xy-plane and in z-direction.

One effective way in analytic expression for the equilibrium properties of the system is to solve the GP equation based on a certain variational ansatz. Simple ansatz using Heaviside step function [21] or linear function [22] to coarsely approximate the density distribution within the vortex core have been used to study vortex properties in rotating BECs. While these early investigation remain in the regime of Wigner-Seitz approximation (round the lattice cells), a better ansatz using tanh function to approximate the variation of density near the vortex

[a] e-mail: ylma@fudan.ac.cn

core [20] was shown to be capable of studying the actual configuration in 2D. An extend numerical work provided a mathematical framework [45]. Our present work will inherit this intuitive ansatz and extend the originally 2D results to a finite 3D system with finite number of vortices and finite bent vortex lengths. In other words, our system is confined in an ellipsoidal harmonic oscillatory trap with trapping potentials in three directions, instead of a flat trap with much stronger trapping potential along z-axis. Both finite size effect along z-direction and the bending of vortices will affect the configuration of vortices on the xy-plane, which is unique for 3D case. Within the condensate region, we take the vortex lines as curved segments along the z-axis with different lengths, core widths and curvature at different positions on the xy-plane. We consider BEC at zero temperature in the Thomas-Fermi (TF) regime, where the interaction energy is very large compared to the external trap potential. The condensate is rotated at varying angular frequencies Ω. At relatively small Ω, the condensate contains several vortices and we are able to determine their actual number and configuration by comparing the different local energy minimum of the different structures. For a greater Ω corresponding to a larger number of vortices ($\approx 10^2$), it is difficult to determine the actual configuration. The amount of calculation grow in a geometric order with vortex numbers, which prevents the intervortex separation and curvature to be determined self-consistently.

By carrying out the finite-N_v calculation including the finite-size effect both in the xy-plane and in the axis of rotation z, it is shown that (1) configurations take the simplest regular polynomial shape in the case of several vortices; (2) triangular "unit cells" are energetically more stable than square "unit cells" regardless of other conditions for the same number of vortices at large enough rotation frequency; (3) bending vortex lines become energetically favorable, and the vortex configuration in the xy-plane has slight expands with the increase of z, especially, when $\lambda < 1$ where the bending first increases and then decreases with increasing rotation frequency; (4) the boundary effect of the condensate causes significant decrease in vortex density than estimated with the infinite boundary, the decrease is less significant when bending of vortex line is considered [52], and the vortex core width first decreases and then increases with increasing rotation frequency [21,22]; (5) plot of N_v vs. Ω agree well with numerical simulations.

The arrangement of the paper is as follows. We take in Section 2 an ansatz for wave function of the BEC and derive analytically the energy function including the self energy and interaction energy of the vortices by using a variational method. In Section 3 we calculate the minimal energy with different structures to determine self-consistently the number of vortices N_v, vortex configurations, intervortex separation b, vortex curvature k_j, and vortex core half-width ξ as a function of drive force Ω, all of which coincide with the numerical simulations with adjustable stirring angular frequency Ω. In Section 4 we end with a conclusion.

2 Model and method

The Hamiltonian density of a rotating trapped BEC can be given by

$$\hat{\mathcal{H}} = \frac{1}{2M}|(-i\hbar\nabla - M\mathbf{\Omega}\times\mathbf{r})\Psi(\mathbf{r})|^2 + [U_{ext}(\mathbf{r}) - \frac{1}{2}M\Omega^2 s^2 - \mu]|\Psi(\mathbf{r})|^2 + \frac{1}{2}g|\Psi(\mathbf{r})|^4. \quad (1)$$

The trapping potential $U_{ext}(\mathbf{r}) = \frac{1}{2}M\omega_\perp^2(s^2+\lambda^2 z^2)$ for spherical trap ($\lambda = 1$) and ellipsoidal trap ($\lambda \neq 1$). The interaction between bosons is described through the coupling constant g related to the s-wave scattering length a_{sc} in the form $g = 4\pi\hbar^2 a_{sc}/M$.

A Heaviside step function [21] or linear function [22] for the density distribution $|\Psi(\mathbf{r})|^2$ within the vortex core is too simple to describe the system. We adopt an ansatz constructed by Castin et al. [20] in which the density is

$$|\Psi(\mathbf{r})|^2 = |\Psi_{slow}(\mathbf{r})|^2 \prod_{j=1}^{N_v} \tanh^2 \frac{|\mathbf{s}-\mathbf{s}_j|}{\xi_j}. \quad (2)$$

Here $\mathbf{s}_j$ is the position of the jth vortex on the xy-plane and ξ_j is the half-width of the vortex core and are both introduced as variational parameters. $|\Psi_{slow}(\mathbf{r})|^2 \cong \frac{\mu_0}{g}(1-\bar{s}^2-\bar{z}^2)$ is the TF density of BEC with 0-vortex [21], which appears to be a slow varying envelope. Here the dimensionless coordinates $\bar{s} \equiv \frac{s}{R_\perp}$ and $\bar{z} \equiv \frac{z}{R_z}$ are in units of TF radius of the condensate: $R_{TF} = [2\mu/(M\omega_\perp^2)]^{1/2}$, $R_\perp = R_{TF}/(1-Q^2)^{1/2}$ and $R_z = R_{TF}/\lambda$. $Q = \Omega/\omega_\perp$ is the rotation frequency in unit of $\omega_\perp$. μ is related to both the bending of the vortex and the chemical potential of BEC with no vortex μ_0, as is shown below in equation (3). From the normalization condition $N = \int \mathrm{d}^3\mathbf{r}|\Psi(\mathbf{r})|^2$ we have $\mu_0 = \frac{1}{2}\hbar\omega_\perp(15\lambda P)^{2/5}$. $P = Na_{sc}/a_{ho}$ is the dimensionless interaction parameter. $a_{ho} = \sqrt{\hbar/M\omega_\perp}$ is the trapping characteristic length. In the TF regime the number of particles N forming the condensate approaches infinitely large, the interaction between particles is dominant as compared to the trap potential. Since $a_{sc}/a_{ho} \simeq 10^{-4}$ in most experiments, P should be a finite large number.

By introducing the curvature of the j'th vortex k_j, the bending vortex line can be described with the vortex displacement field $\mathbf{u}(\mathbf{r})$, indicating the derivation of vortex from its original position: $u(r) = \frac{R_z}{K_j}(1-\sqrt{1-K_j^2\bar{z}^2})$ for the axial symmetrical system $\mathbf{u}(\mathbf{r}) = (\hat{x}+\hat{y})u(\mathbf{r})$, where $K_j = k_j R_z$ are independent on $\mathbf{r}$ when $u(r) \ll R_{TF}$. The general form of the phase ϕ is $\phi = \phi_0 + \sum_{j=1}^{N_v}(k_j s\varphi + \theta_j)$, where θ_j are the relative polar angle of a system of Cartesian coordinates centered on the vortex core, φ is the polar angle of the system centered on the trapping center, and ϕ_0 is the single value part of the phase. For axial symmetry, $\phi_0 = 0$. We will see below that the bending vortices are more stable than straight vortices when $\lambda < 1$ and that the phase shift $k_j s\varphi$ will play an important role in

lowering the total vortex energy. For small vortex displacement field $\mathbf{u}(\mathbf{r})$ and for $\xi_j \ll b$, the bending can be viewed as elastic deformation, thus the vortex line bending tension is [53] $\tau = \hbar\Omega|\Psi(\mathbf{r})|^2 \ln\frac{a_\Omega}{\xi}$ with $a_\Omega = \sqrt{\hbar/M\Omega}$ and the corresponding elastic energy has a simple form [54,55] $\epsilon_{el}(\mathbf{r}) = \tau(\frac{\partial u}{\partial z})^2$. By adding this elastic energy term to the Hamiltonian (1), and substituting the trial wave function (2), we obtain the chemical potential

$$\mu = \mu_0\left[1 - 5(\ln 2)\sum_{j=1}^{N_v}\gamma_j\bar{\xi}_j^2(1-\bar{s}_j^2)^{3/2}\right]^{-2/5}. \quad (3)$$

In the deduction of equation (3) we have used the position of the vortex $\bar{s}_j = \frac{s_j}{R_\perp}$ and radius of the vortex $\bar{\xi}_j = \frac{\xi_j}{R_\perp}$ in units of TF radius of the condensate in the xy-plane. The dimensionless parameter defined as $\gamma_j = (1 + K_j^2\frac{\hbar\Omega}{\mu}\ln\frac{a_\Omega}{\xi})^{-1/2}$ returns to $\gamma_j = 1$ of the straight vortex line for $k_j = 0$. The normalization integration and hence the energy integration below are carried out within the ellipsoid of $\bar{s}^2 + \gamma_j^{-2}\bar{z}^2 \le 1$ when taking into account both the finite-size effect and the bending effect.

By separating the phase and modulus of the wavefunction in equation (1) with elastic energy added, one obtains

$$\begin{aligned}\hat{\mathcal{H}} = \sum_{j=1}^{N_v}\Big\{&\frac{\hbar^2}{2M}|\Psi(\mathbf{r})|^2\Big[|\nabla_j\ln|\Psi(\mathbf{r})||^2 + |\nabla\theta_j|^2\\ &+k_j\Big(k_j + \frac{2}{s}\frac{\partial\theta_j}{\partial\varphi}\Big) + \sum_{j'\neq j}^{N_v}(\nabla\theta_j)\cdot(\nabla\theta_{j'})\Big]\\ &-\hbar\Omega|\Psi(\mathbf{r})|^2\Big[\frac{\partial\theta_j}{\partial\varphi} - \Big(\frac{\partial u}{\partial z}\Big)^2\ln\frac{a_\Omega}{\xi} + k_j s\Big]\\ &+[U_{ext}(\mathbf{r}) - \mu]|\Psi(\mathbf{r})|^2 + \frac{1}{2}g|\Psi(\mathbf{r})|^4\Big\}. \quad (4)\end{aligned}$$

By substituting the ansatz (Eq. (2)) into equation (4), we calculate the total energy of the system per particle in the form $E = \mu_0 + \sum_{j=1}^{N_v}W(s_j) + \sum_{j\neq j'=1}^{N_v}V(s_j, s_{j'})$. Here the self energy of the system $W(s_j)$ is obtained through integrating the jth vortex in the Hamiltonian density equation (4), and the interaction energy $V(s_j, s_{j'})$ between the jth and the j'th vortex comes from the crossover term $\sum_{j'\neq j}^{N_v}(\nabla\theta_j)\cdot(\nabla\theta_{j'})$. The integration of the term $|\nabla\theta_j|^2$ diverges at the center of the vortex. The usual cutoff is at $\bar{s} = \bar{s}_j + \alpha\bar{\xi}_j$. The parameter α should be chosen to be self-consistent with the cutoff effect in the different positions of the vortices. Since $0 < \bar{\xi}_j \ll 1$, the cutoff requires usually $\alpha\bar{\xi}_j \ll 1$ for $\bar{s}_j < 1$. But for $\bar{s}_j \lesssim 1$ the position of outside vortices is nearest to the boundary of the condensate when the vortices fill the whole xy-plane, the cutoff requires $0 < \alpha \ll 1$ in a self-consistent manner. Different values of α in this region will have some slight impact on the results but do not alter the main characteristics of the system.

Carrying out the integral within the ellipsoid by use of the cutoff, the self-energy $W(s_j)$ can be written as

$$\begin{aligned}W(s_j) = &\frac{\hbar\omega_\perp\gamma_j}{6\lambda P}\left(\frac{2\mu}{\hbar\omega_\perp}\right)^{3/2}\Bigg\{\frac{4}{3} - \bar{s}_j^2\\ &+ (1-\bar{s}_j^2)^{3/2}\left[\frac{1}{3}\ln 2 - \frac{5}{2} - \ln\frac{1+\sqrt{1-\bar{s}_j^2}}{2(1-\bar{s}_j^2)}\alpha\bar{\xi}_j^2\right]\Bigg\}\\ &+ \frac{10\mu^2\gamma_j}{\hbar\omega_\perp}\left(\frac{\mu}{\mu_0}\right)^{\frac{3}{2}}\left[\frac{15\lambda P}{1-Q^2}\right]^{-\frac{2}{5}}\\ &\times\Bigg\{\bar{\xi}_j^2(1-\bar{s}_j^2)^{\frac{3}{2}}\frac{\ln 2}{1-Q^2} + \bar{\xi}_j^2(1-\bar{s}_j^2)^{\frac{5}{2}}\Bigg[\frac{4\ln 2 - 1}{15}\\ &+ \frac{\ln 2}{5\lambda^2} - \frac{\ln 2}{1-Q^2}\Bigg]\Bigg\} - \hbar\Omega\gamma_j(\frac{\mu}{\mu_0})^{5/2}(1-\bar{s}_j^2)^{5/2}\\ &+ \gamma_j\Bigg[\frac{5(\hbar\omega_\perp)^2\sqrt{1-Q^2}K_jI_j}{8\mu} + \lambda^2K_j^2\frac{(\hbar\omega_\perp)^2}{4\mu}\\ &- \frac{5\pi}{128}\frac{K_j\hbar\Omega}{\sqrt{1-Q^2}}\Bigg] + \frac{15}{8}\hbar\omega_\perp\frac{Q}{1-Q^2}\ln\left(\frac{a_\Omega}{\xi_j}\right)J_j, \quad (5)\end{aligned}$$

in which $I_j \equiv \int_{\arcsin\bar{s}_j}^{\frac{\pi}{2}}\cos^4\varphi\mathrm{d}\varphi$ and $J_j \equiv \frac{1}{2K_j}[(1 - \frac{1}{c_j^2})^2(\mathrm{arctanh}c_j - c_j) + \frac{7c_j}{15} - \frac{1}{3c_j}]$ with $c_j = K_j\gamma_j$. Note that $J_j \simeq \frac{1}{2}\gamma_j(\frac{1}{3}c_j^2 - \frac{1}{5})$ for $c_j \to 0$. The term $-\frac{5\pi}{128}\frac{\hbar\Omega}{\sqrt{1-Q^2}}K_j\gamma_j$ in equation (5) coming from the term $-\hbar\Omega|\Psi(\mathbf{r})|^2k_js$ in equation (4) dominates the bending originally from the phase shift of $k_js\varphi$.

By carefully handling the integral of the interaction term, the explicit expression for the interaction energy $V(s_j, s_{j'})$ is

$$\begin{aligned}V(s_j, s_{j'}) = &-\hbar\omega_\perp\gamma_j(1-Q^2)^{3/5}\frac{5(\mu/\mu_0)^{3/2}}{2(15\lambda P)^{2/5}}\\ &\times\Bigg\{\Bigg[2\rho_j\left(\frac{1}{3}\rho_j^2 + f_r\right)\\ &-\left(\frac{1}{3} + f_r\right) + \frac{I_{jj'}}{\bar{s}_j\bar{s}_{j'}\sin\theta_{jj'}}\Bigg] + \Bigg[2\rho_{j'}\left(\frac{1}{3}\rho_{j'}^2 + f_r\right)\\ &-\left(\frac{1}{3} + f_r\right) + \frac{I_{j'j}}{\bar{s}_j\bar{s}_{j'}\sin\theta_{jj'}}\Bigg]\Bigg\}. \quad (6)\end{aligned}$$

Here $\rho_j \equiv \sqrt{1-\bar{s}_j^2}$, $f \equiv 1 - \bar{s}_j\bar{s}_{j'}e^{-i\theta_{jj'}}$, $f_r = \mathrm{Re}\,f$ and $f_i = \mathrm{Im}\,f$, and $\theta_{jj'}$ is the angle between the vectors $\mathbf{s}_j$ and $\mathbf{s}_{j'}$. Taking $\varphi_{jj'} \equiv \arctan\frac{\bar{s}_j\bar{s}_{j'}\sin\theta_{jj'}}{1-\bar{s}_j\bar{s}_{j'}\cos\theta_{jj'}}$ and letting

$$\begin{aligned}X_\pm \equiv \Big[&\pm\rho_j^2 - \rho_j(2-\rho_j)\sqrt{|f|}\cos\frac{\varphi_{jj'}}{2}\\ &\pm(1-2\rho_j)\,|f|\cos\varphi_{jj'} + |f|^{\frac{3}{2}}\cos\frac{3\varphi_{jj'}}{2}\Big]\end{aligned}$$

and

$$\begin{aligned}Y_\pm \equiv \Big[&-\rho_j(2-\rho_j)\sqrt{|f|}\sin\frac{\varphi_{jj'}}{2}\\ &\pm(1-2\rho_j)\,|f|\sin\varphi_{jj'} + |f|^{\frac{3}{2}}\sin\frac{3\varphi_{jj'}}{2}\Big],\end{aligned}$$

$I_{jj'}$ has the form

$$I_{jj'} \equiv \frac{1}{2}\sqrt{|f|}\Big\{(f_r^2 - {f_i}^2 + |f|f_r) \times \Big(\sin\frac{\varphi_{jj'}}{2}\Big)\ln\sqrt{\frac{X_+^2+Y_+^2}{X_-^2+Y_-^2}} + (f_r^2 - {f_i}^2 - |f|f_r) \times \Big(\cos\frac{\varphi_{jj'}}{2}\Big)\Big(\arctan\frac{Y_+}{X_+} - \arctan\frac{Y_-}{X_-}\Big)\Big\}. \quad (7)$$

Because of the finite-size effect of the ellipsoidal trap, equation (6) is much more complicated than equation (67) in [20]. In two special cases, equation(6) takes a simpler form:

(i) for $\theta_{jj'} = 0$ or $\theta_{jj'} = \pi$, i.e., the two position vectors pointing to the two vortices considered are in the same or opposite direction,

$$V_{line}(s_j, s_{j'}) = -\hbar\omega_\perp\gamma_j(1-Q^2)^{3/5}\frac{5(\mu/\mu_0)^{3/2}}{2(15\lambda P)^{2/5}} \times \Big\{-2(\frac{1}{3}+f)+2f(\rho_j+\rho_{j'})+\frac{2}{3}(\rho_j^3+\rho_{j'}^3) + f^{\frac{3}{2}}\ln\Big[\frac{\sqrt{f}-\rho_j}{\sqrt{f}+\rho_j}\frac{\sqrt{f}-\rho_{j'}}{\sqrt{f}+\rho_{j'}}\frac{1+\sqrt{f}}{1-\sqrt{f}}\Big]\Big\} \quad (8)$$

with $f = 1 - \bar{s}_j\bar{s}_{j'}$;

(ii) for $\bar{s}_{j'} = 0$, i.e., when one of the two vortices is located at the center of the BEC,

$$V(s_j, 0) = -\hbar\omega_\perp\gamma_j(1-Q^2)^{3/5}\frac{5(\mu/\mu_0)^{3/2}}{2(15\lambda P)^{2/5}} \times \Big[\frac{2}{3}(4-\bar{s}_j^2)\sqrt{1-\bar{s}_j^2} + \ln\frac{1-\sqrt{1-\bar{s}_j^2}}{1+\sqrt{1-\bar{s}_j^2}}\Big]. \quad (9)$$

With the explicit expression of the total energy E, we are, in principle, able to evaluate the values of jth vortex k_j and ξ_j through

$$\frac{\partial E}{\partial(k_j,\xi_j)} = 0, \quad \frac{\partial^2 E}{\partial(k_j,\xi_j)^2} > 0. \quad (10)$$

From equation (3), the chemical potential μ can only be determined after the k_j and ξ_j of every vortex are determined beforehand. Therefore the calculation is to solve an "integral equation with unknown upper integral limit" N_v. The minimal energy function by a drive force Q depends on the number of vortices N_v, vortex configurations, intervortex separation b, vortex core half-width ξ_j, and the bending related parameter γ_j after carrying out the self-consistent calculation on chemical potential μ. By assuming the dimensionless curvature of the vortex lattice is K through the curvature $k_j = K\bar{s}_j/R_z$, one has $u(r_j) \simeq \frac{1}{2}R_zK\bar{s}_j\bar{z}_j^2$. This means that bending of vortex occurs at the boundary of the condensate. In the next section we will calculate the minimal Gross-Pitaevskii energy $E(N_v, b, k_j, \xi_j)$ variationally as a function of Ω.

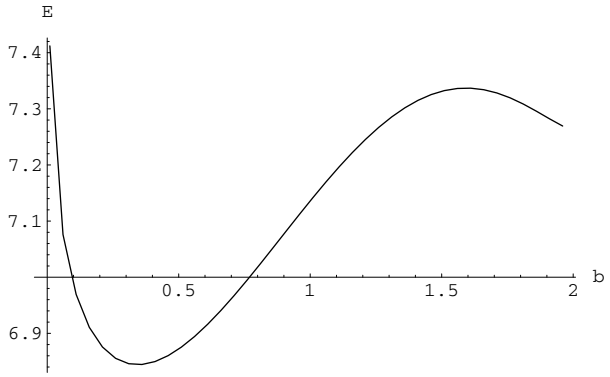

Fig. 1. The total energy E in unit of $\hbar\omega_\perp$ vs. the distance b in unit of $R_\perp$ with $Q = 0.47$, $\lambda = 1$ and $P = 100$.

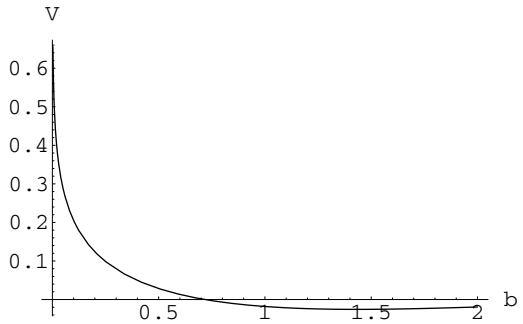

Fig. 2. The interaction energy V in unit of $\hbar\omega_\perp$ vs. the distance b in unit of $R_\perp$ between two symmetrically placed vortex with $Q = 0.47$, $\lambda = 1$ and $P = 100$.

3 Results and discussion

Most experimental observation of vortex lattices are generated within a condensate of moderate number of particles, therefore in the following calculation, we take $P = 100, 500, 1000$ respectively in most cases. Forming a vortex lattice requires, in principle, that a unit cell be infinitely replicated. In our case with finite number of vortices and finite condensate size, the concept of vortex lattice is a good approximation for the large number of vortices.

Since we account for the interaction energy of every two of the vortices, the amount of calculation grow in a geometric order with vortex number. To cope with this difficulty, we first look into the case with several vortices for which the concept of lattice is barely relevant but the calculation is simple, and thus can be studied more carefully in the whole parameter range. We then study the change in vortex number to the increase of rotation frequency at fixed configuration of hexagonal unit cells for the large and finite number of vortices in the small parameter range.

Curves in Figures 1 and 2 show the total energy E and interaction energy V as a function of the distance between two straight vortices that are symmetrically displaced by $b/2$ from the trap center. The self-energy W dominates the steady state configuration. The minimizers of E correspond to a series of N_v, b and ξ_j for changing the values of Q. When placed close enough the interaction diverges logarithmically, at a finite distance the interaction

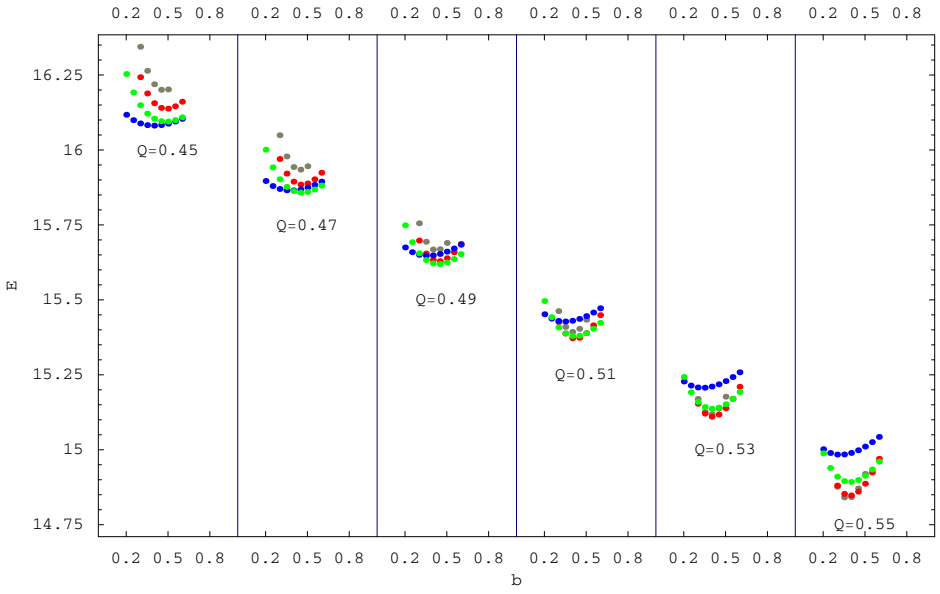

Fig. 3. (Color online) Local energy (near minima) in unit of $\hbar\omega_\perp$ vs. the distance b in unit of $R_\perp$ with $\lambda = 1$, $P = 500$, and $N_v = 2$ (blue), 3 (green), 4 (red), 5 (gray) in the different driving forces Q.

is purely repulsive, and to cross over a certain distance apart the interaction turns into slightly attractive due to the boundary effect.

3.1 The critical frequencies ($N_v = 1$)

The critical frequency Ω_c is defined as the rotation frequency above which the single vortex solution has an energy lower than the condensate without vortex[20]. From the condition $W = 0$ at $\bar{s}_j = 0$ we get $\Omega_c/\omega_\perp = (5\mu_0/6\mu)(15\lambda P)^{-2/5}[3\ln(2/\alpha\bar{\xi}) - 2 + \ln 2]$ and calculate $\Omega_c/\omega_\perp = 0.520, 0.352, 0.289$ for $P = 100, 500, 1000$ respectively. Another frequency suggested in [20] is Ω_{stab} above which the vortex is a local minimum of energy, calculated from the condition $dW/d\bar{s}_j = 0$ at $\bar{s}_j = 0$. That is $\Omega_{stab}/\omega_\perp = (\mu_0/2\mu)(15\lambda P)^{-2/5}[3\ln(1/\alpha\bar{\xi}) - 5/2 + \ln 2]$ and has values $\Omega_{stab}/\omega_\perp = 0.346, 0.217, 0.175$ for $P = 100, 500, 1000$ respectively. $\Omega_{stab} = (3/5)\Omega_c$ in the limit of $\alpha\bar{\xi} \to 0$ is estimated the same as predicted [12]. The critical frequencies are very close to the values in [20,45].

3.2 Case with several vortices ($N_v = 2$–7)

The local energy minimum of the system with N_v vortices under a certain rotation frequency Q is obtained through a three dimensional variation calculation. The variation parameters are the separation of the vortices in the TF units $\bar{b}$, the vortex curvature k and the core width ξ. Since we consider only the regular vortex lattice structure, the positions of the vortices are totally determined by their separation. Local energy minimum of the system with the different number of vortices (from 2 to 7) are compared and the lowest one is the global energy minimum of the system, which determines the actual vortex number, configuration, and curvature of the BEC under the given rotation frequency Q.

In order to determine the number of vortices in a condensate under different driving frequencies Q, we plot in Figure 3 the total energy of the system to the distance between vortices $\bar{b}$ with $N_v = 2, 3, 4, 5$ under different value of driving frequencies Q. The curves formed by dots of the same color show the energy of the system at discrete values of $\bar{b}$. Dots with different color indicate different vortex numbers, and every separation 'deck' of dotted curves correspond to a system under a single Q. Therefore the color of the lowest dots (global energy minimum) of every 'deck' tells both the number of vortices contained in the actual BEC rotating under frequency $\Omega = Q\omega_\perp$ and determines self-consistently the intervortex separation in a fixed configuration. By repeating the above procedure under a series of increasing rotation frequency Q, we find that the vortices are generated one by one with the increase of Q. Moreover, for the local energy minimum of the system containing N_v vortices, only when it is also the global energy minimum of the system, can it be lower than the local energy minimum of the system with either $N_v - 1$ or $N_v + 1$ vortices.

For cases with more than three vortices, since that the external trap and stirring perturbation are axial symmetric, only two different regular configurations are allowed, as shown in Figures 4–7. From Figures 4, 5 and 6 for $N_v = 4$, 5 and 6, it was shown that the configuration with one vortex in the center and others on a circle around always posses a slightly higher local minimum energy with the same values of P regardless of the values of Q. The stable configuration is such that except for the case of one vortex, no vortex will appear in the center of the trap if the condensate holds less than seven vortices.

For $N_v = 7$, however, the configuration with a vortex in the center, which forms a hexagonal shape as shown in Figure 7 (right), posses a lower local energy minimum compared with the configuration of seven vortices on a circle as shown in Figure 7 (left). The stable configurations

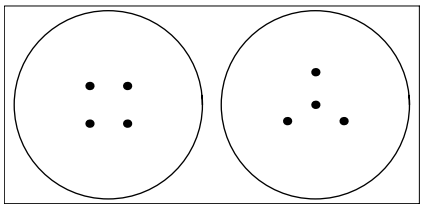

Fig. 4. Left: four vortices forming a square. Right: one vortex in the center and three vortices forming an equilateral triangle. Energy difference between left and right $\Delta E = E_L - E_R = -0.031\hbar\omega_\perp$ with $\lambda = 1$, $P = 500$ and $Q = 0.26$.

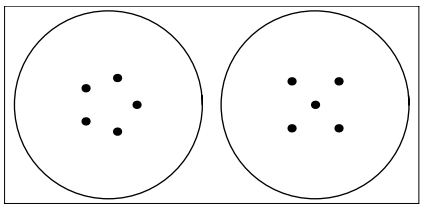

Fig. 5. Left: five vortices forming a pentagonal lattice. Right: one vortex in the center and four vortices forming a square. Energy difference between left and right $\Delta E = -0.029\hbar\omega_\perp$ with $\lambda = 1$, $P = 500$ and $Q = 0.29$.

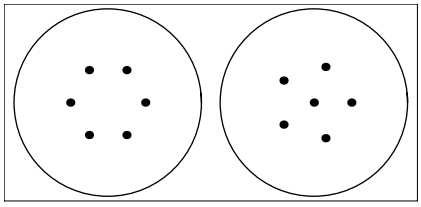

Fig. 6. Left: six vortices forming a hexagonal lattice. Right: one vortex in the center and three vortices forming an equilateral triangle. Energy difference between left and right $\Delta E = -0.122\hbar\omega_\perp$ with $\lambda = 1$, $P = 500$ and $Q = 0.35$.

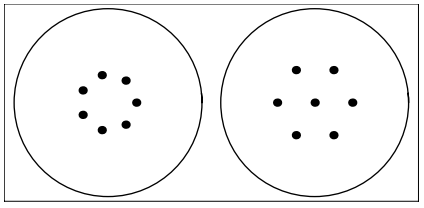

Fig. 7. Left: seven vortices on a circle. Right: one vortex in the center and six vortices in a hexagonal lattice. Energy difference between left and right $\Delta E = +0.016\hbar\omega_\perp$ with $\lambda = 1$, $P = 500$ and $Q = 0.61$.

imply that vortices in the equilibrium state will form regular polynomial cells with the least vortices involved.

3.3 Case with many vortices ($N_v \geq 10$)

We assume that the relation between the local energy minimum and global minimum of the system is also true for the larger number of vortices. Therefore we are able to determine the vortex number N_v of the system by comparing it with $N_v - 1$ and $N_v + 1$ vortices without considering other vortex numbers (however, the curvature k_j and core width ξ_j are self-consistently calculated), which will save time in the amount of calculation.

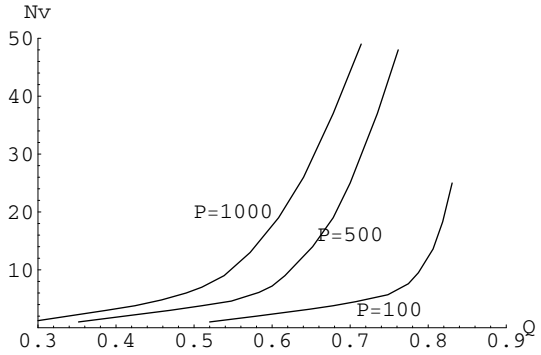

Fig. 8. Estimated number of vortices in BECs vs. the rotation frequency Q with $\lambda = 1$, $P = 100, 500, 1000$.

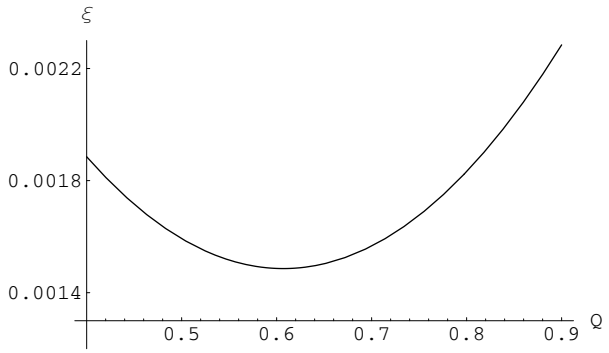

Fig. 9. The average vortex core width ξ in unit of $R_\perp$ vs. the rotation frequency Q with $\lambda = 1$, $P = 500$.

For a final stable static state, we are limited to calculating BECs with only a few particular number of vortices that will completely fit into a lattice. We study only the triangular lattices, to approximate for the actual situation while taking into account the effects of finite numbers of vortices, finite size and small bending. Through comparing the local energy minimum of different numbers of vortices in the condensate, we plot the estimated number of vortices as a function of Q with several different P in Figure 8. This result coincide with the experiments [9] and numerical results [36,54]. Apparently it is easier to create more vortices under the same rotation frequency in larger condensates.

In Figure 9 we show the variation of the average half-width of vortex cores ξ in unit of $R_\perp$ versus the rotation frequency Q. The decrease of ξ with increasing Q when Q is small is expected as usual tendency. However, the increase of ξ with increasing Q when Q is large shows the impact of boundary effect, when the area occupied by the total lattice structure became comparable with the total surface area. In other words, the vortex half width ξ tends to increase with increasing N_v/N, the ratio of the numbers of vortices N_v to particles N, when the vortices extend to the edge of the condensate where the particle density is much smaller. Moreover, both finite number of vortices

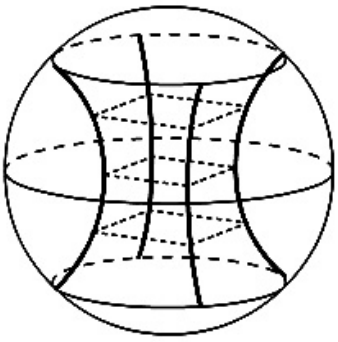

Fig. 10. Four bent vortices forming a square unit cell on the xy-plane. At $\lambda = 1/2$, $P = 500$ and $Q = 0.18$, the separation between the nearest vortices on $(z = 0)$-plane is $\bar{b} = 0.75$ with the dimensionless curvature $K = 0.757$ and total energy $E = 12.45\hbar\omega_\perp$.

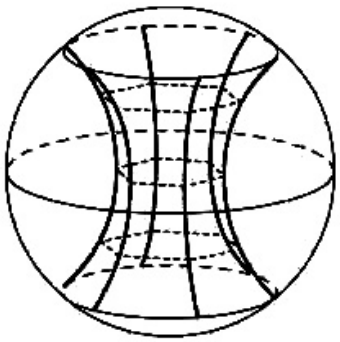

Fig. 11. Six bent vortices forming a hexagonal unit cell on the xy-plane. At $\lambda = 1/2$, $P = 500$ and $Q = 0.24$, the separation between the nearest vortices on $(z = 0)$-plane is $\bar{b} = 0.71$ with the dimensionless curvature $K = 1.053$ and total energy $E = 12.30\hbar\omega_\perp$.

and boundary effect always leads to $N_v < \lfloor R_\perp^2/b^2 \rfloor$ in the minimal energy calculation.

3.4 Effects of the bending

In order for the energy of the system to be minimized, vortices in a trapped condensate should adopt a non zero curvature on z-direction, i.e. bending vortices are energetically more favorable than straight ones in same cases. In Figures 10 and 11 we plot the case of four and six vortices forming a square and a hexagon unit cell respectively, in both cases the vortices bent at a certain curvature k_j calculated self-consistently. Moreover, the close stack of the vortices around the center of the trap as shown below agrees with the one simulated in [20] but disagrees with one simulated in [36] which may be caused by not arriving completely at the equilibrium state. Although when we study bent vortices, their separation b is slightly greater than straight ones, it still gives $N_v < \lfloor R_\perp^2/b^2 \rfloor$, an effect of finite number of vortices and finite size. The expand is similar with the result in [56].

We also show through our calculation that bent vortex lines are still more energetically favorable than straight ones for $\lambda < 1$ (as shown in Fig. 12 for $\lambda = 1/2$), and triangular unit cells are more energetically favorable than square cells (not be shown).

The curvature of the jth vortex is $k_j = K_j \bar{s}_j / R_z$ and the mean dimensionless curvature of vortex lines is $K = \frac{1}{L_v} \sum_{j=1}^{L_v} K_j$ with L_v the layer number of the vortex lattice around the trapping center. In Figure 13 we show the variation of the mean dimensionless curvature of vortex lines K versus the rotation frequency Q. The

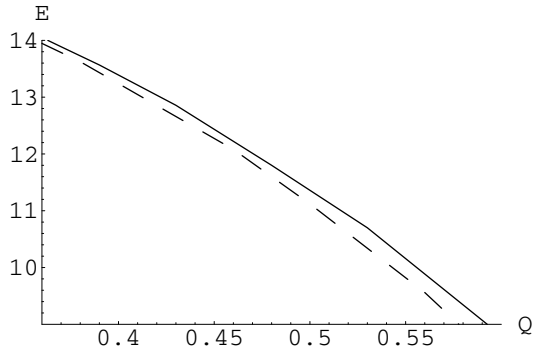

Fig. 12. Energy of rotating BEC with vortices in unit of $\hbar\omega_\perp$ vs. rotation frequency Q with $\lambda = 1/2$, $P = 500$. The solid line stands for straight vortices and the dashed line stands for bent ones.

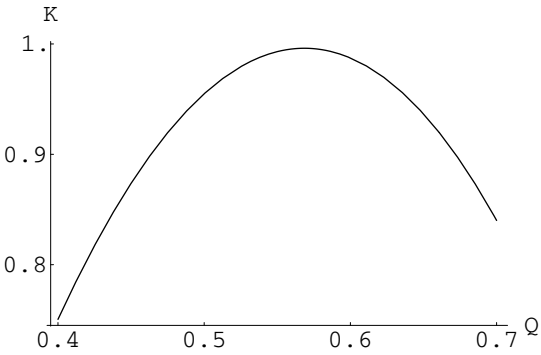

Fig. 13. The dimensionless curvature of vortex lines K vs. the rotation frequency Q with $\lambda = 1/2$, $P = 500$.

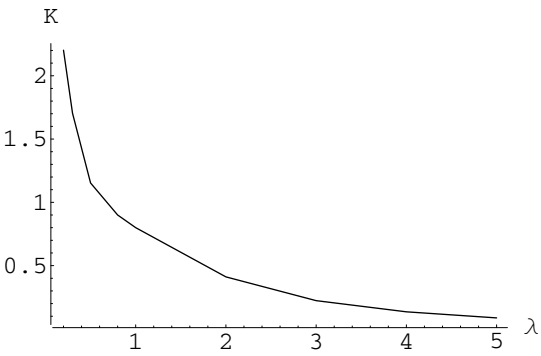

Fig. 14. The dimensionless curvature of vortex lines K vs. the ratio λ with $P = 500$, $Q = 0.24$ and $N_v = 6$.

curvature K first increases and then decreases with the increasing of Q within the range of calculation. This indicates that straight vortex lines are only good approximation when the number of vortices both is a few and is large enough. Of course, the vortex bending occurs at the boundary where both is the end of the vortex line and is the maximum value of $\bar{s}_j$.

Curve in Figure 14 shows the monotonic decrease of the curvature K with the increasing of λ. This agrees with the numerical[43] and analytical [44,46,51] results.

4 Conclusion

We have studied the vortex formation in a three dimensional Bose-Einstein condensate using a simple variational ansatz, emphasizing on the curvature, finite number and size of vortices. We have calculated the minimal energy configurations of the vortices as a function of the rotation frequency and obtained the number of vortices, three-dimensional configuration and curvature of vortex lines in a self-consistent manner. The effect of finite number of vortices and finite size shows that the calculated vortex number is less than one would estimate from the ratio of the xy-plane area to single vortex area shared in the xy-plane. The slight expansion of vortex lattice caused by vortex bending for $\lambda < 1$ decreases the difference between the two.

Our results have explained the experimental observation of bending vortex lines and triangular vortex lattice. Our method proves an effective and simple tool to approximately determine certain important behavior of the system such as the number of vortices, their curvature and configurations under different rotation frequencies when taking into account the effects of number and shape of the vortex lines. Further theoretical study of vortex lattice formation and periodic solution of the Gross-Pitaevskii equation in a three dimensional confined rotating Bose-Einstein condensate is in progress.

We thank Mr. Wei Zhou for helping to plot two 3D graphics. This work was supported by the National Natural Science Foundation of China under Grant Nos. 10274012 and 10574028.

References

1. M.R. Matthews et al., Phys. Rev. Lett. **83**, 2498 (1999)
2. K.W. Madison, F. Chevy, W. Wohlleben, J. Dalibard, Phys. Rev. Lett. **84**, 806 (2000)
3. B.P. Anderson, P.C. Haljan, C.E. Wieman, E.A. Cornell, Phys. Rev. Lett. **85**, 2857 (2000)
4. E. Hodby, G. Hechenblaikner, S.A. Hopkins, O.M. Maragó, C.J. Foot, Phys. Rev. Lett. **88**, 010405 (2002)
5. B.P. Anderson et al., Phys. Rev. Lett. **86**, 2926 (2001)
6. Z. Dutton, M. Budde, C. Slowe, L.V. Hau, Science **293**, 663 (2001)
7. K.W. Madison, F. Chevy, V. Bretin, J. Dalibard, Phys. Rev. Lett. **86**, 4443 (2001)
8. P.C. Haljan, I. Coddington, P. Engels, E.A. Cornell, Phys. Rev. Lett. **87**, 210403 (2001)
9. J.R. Abo-Shaeer, C. Raman, J.M. Vogels, W. Ketterle, Science **292**, 476 (2001)
10. P. Engels, I. Coddington, P.C. Haljan, V. Schweikhard, E. A. Cornell, Phys. Rev. Lett. **90**, 170405 (2003)
11. I. Coddington, P. Engels, V. Schweikhard, E.A. Cornell, Phys. Rev. Lett. **91**, 100402 (2003)
12. A.L. Fetter, A.A. Svidzinsky, J. Phys.: Condens. Matter **13**, R135 (2001)
13. A.J. Leggett, Rev. Mod. Phys. **73**, 307 (2001)
14. D.S. Rokhsar, Phys. Rev. Lett. **79**, 2164 (1997)
15. A.A. Svidzinsky, A.L. Fetter, Phys. Rev. A **58**, 3168 (1998)
16. A.L. Fetter, J. Low Temp. Phys. **113**, 189 (1998)
17. F. Dalfovo, S. Stringari, Phys. Rev. A **53**, 2477 (1996)
18. R.J. Dodd, K. Burnett, M. Edwards, C.W. Clark, Phys. Rev. A **56**, 587 (1997)
19. J.J. García-Ripoll, V.M. Pérez-García, Phys. Rev. A **60**, 4864 (1999)
20. Y. Castin, R. Dum, Eur. Phys. J. D **7**, 399 (1999)
21. A.L. Fetter, Phys. Rev. A **64**, 063608 (2001)
22. U.R. Fischer, G. Baym, Phys. Rev. Lett. **90**, 140402 (2003)
23. T.-L. Ho, Phys. Rev. Lett. **87**, 060403 (2001)
24. M. Cozzini, S. Stringari, Phys. Rev. A **67**, 041602(R) (2003)
25. G. Baym, Phys. Rev. Lett. **91**, 110402 (2003)
26. D.A. Butts, D.S. Rokshar, Nature **397**, 327(1999)
27. E.J. Mueller, T.-L. Ho, Phys. Rev. Lett. **88**, 180403 (2002)
28. T. Kita, T. Mizushima, K. Machida, Phys. Rev. A **66**, 061601(R) (2002)
29. K. Kasamatsu, M. Tsubota, M. Ueda, Phys. Rev. A **66**, 053606 (2002)
30. T.P. Simula, S.M.M. Virtanen, M.M. Salomaa, Phys. Rev. A **65**, 033614 (2002)
31. N.R. Cooper, N.K. Wilkin, J.M.F. Gunn, Phys. Rev. Lett. **87**, 120405 (2001)
32. J. Sinova, C.B. Hanna, A.H. MacDonald, Phys. Rev. Lett. **89**, 030403 (2002)
33. P. Engels, I. Coddington, P.C. Haljan, E.A. Cornell, Phys. Rev. Lett. **89**, 100403 (2002)
34. E.J. Mueller, T-L. Ho, Phys. Rev. A **67**, 063602 (2003)
35. D.L. Feder, A.A. Svidzinsky, A.L. Fetter, C.W. Clark, Phys. Rev. Lett. **86**, 564 (2001)
36. M. Tsubota, K. Kasamatsu, M. Ueda, Phys. Rev. A **65**, 023603 (2002); K. Kasamatsu, M. Tsubota, M. Ueda, Phys. Rev. A **67**, 033610 (2003)
37. A.A. Penckwitt, R.J. Ballagh, C.W. Gardiner, Phys. Rev. Lett. **89**, 260402 (2002)
38. E. Lundh, J.-P. Martikainen, K.-A. Suominen, Phys. Rev. A **67**, 063604 (2003)
39. C. Lobo, A. Sinatra, Y. Castin, Phys. Rev. Lett. **92**, 020403 (2004)
40. P. Rosenbush, V. Bretin, J. Dalibard, Phys. Rev. Lett. **89**, 200403 (2002)
41. V. Bretin, P. Rosenbusch, J. Dalibard, J. Opt. B: Quant. Semiclass. Opt. **5**, S23 (2003)
42. J.J. García-Ripoll, V.M. Pérez-García, Phys. Rev. A **63**, 041603 (2001)
43. A. Aftalion, I. Danaila, Phys. Rev. A **68**, 023603 (2003)
44. A. Aftalion, T. Riviere, Phys. Rev. A **64**, 043611 (2001); A. Aftalion, R.L. Jerrard, Phys. Rev. A **66**, 023611 (2002)
45. A. Aftalion, Q. Du, Phys. Rev. A **64**, 063603 (2001)
46. M. Modugno, L. Pricoupenko, Y. Castin, Eur. Phys. J. D **22**, 235 (2003)
47. G.M. Kavoulakis, Phys. Rev. A **65**, 023602 (2002)
48. M. Linn, M. Niemeyer, A.L. Fetter, Phys. Rev. A **64**, 023602 (2001)
49. D.L. Feder, C.W. Clark, B.I. Schneider, Phys. Rev. A **61**, 011601 (2000)
50. M.Ö. Oktel, Phys. Rev. A **69**, 023618 (2004)
51. A.A. Svidzinsky, A.L. Fetter, Phys. Rev. A **62**, 063617 (2000)
52. D.L. Feder, C.W. Clark, Phys. Rev. Lett. **87**, 190401 (2001)
53. G. Baym, C.J. Pethick, Phys. Rev. A **69**, 043619 (2004)
54. S.A. Gifford, G. Baym, Phys. Rev. A **70**, 033602 (2004)
55. M. Cozzini, L.P. Pitaevskii, S. Stringari, Phys. Rev. Lett. **92**, 220401 (2004)
56. A. Aftalion, X. Blanc, J. Dalibard, Phys. Rev. A **71**, 023611 (2005)